

STELLAR ACTIVITY

Reconciling solar and stellar magnetic cycles with nonlinear dynamo simulations

A. Strugarek,^{1,2*} P. Beaudoin,¹ P. Charbonneau,¹ A. S. Brun,² J.-D. do Nascimento Jr.,^{3,4}

The magnetic fields of solar-type stars are observed to cycle over decadal periods—11 years in the case of the Sun. The fields originate in the turbulent convective layers of stars and have a complex dependency upon stellar rotation rate. We have performed a set of turbulent global simulations that exhibit magnetic cycles varying systematically with stellar rotation and luminosity. We find that the magnetic cycle period is inversely proportional to the Rossby number, which quantifies the influence of rotation on turbulent convection. The trend relies on a fundamentally nonlinear dynamo process and is compatible with the Sun's cycle and those of other solar-type stars.

The characterization of stellar activity and its dynamo origin has broad applications, from exoplanet searches to space weather forecasting. Observational data now allow the determination of absolute luminosities via accurate parallax measurements, rotation through Doppler line broadening and precision photometry, stellar differential rotation through photometry and asteroseismic sounding, and the large-scale spatial structure of stellar photospheric magnetic fields through Zeeman-Doppler imaging. These data complement stellar activity measurements, available from long-term monitoring programs (1, 2), that showed complex variations of stellar cycle amplitudes and periods as a function of fundamental stellar parameters such as mass, luminosity, rotation, and age. The physical understanding of stellar activity is henceforth more complex than suggested by earlier inter-

pretation of stellar cycle data through mean-field dynamo theory (3–5).

Modern global magnetohydrodynamic (MHD) simulations of solar convection and large-scale flows have succeeded in producing, in a self-consistent manner, large-scale magnetic fields (6, 7), in some cases generating regular, solar-like cyclic magnetic polarity reversals (8–11). Thus, these simulations are used today to help our physical interpretation of stellar magnetic cycle observations.

We have performed a set of global MHD simulations with the EULAG-MHD code (12), using a fixed-background stellar structure but covering rotation periods (P_{rot}) between 14 and 29 days and a convective luminosity between 0.2 and 0.6 solar luminosity (table S1). The simulated domain consists of a global (i.e., spherical) stellar convection zone with a solar-like aspect ratio (the radius at the bottom of the spherical shell is

70% of the radius at the top, R_{top}), covering 3.22 density scale-heights with no underlying stable radiation zone. All simulations in the set generate some solar-like features, including (i) an accumulation of a kilo-Gauss, large-scale axisymmetric magnetic field at the bottom of the convection zone; (ii) regular polarity reversals on a decadal time scale, reasonably synchronized across hemispheres; (iii) an equatorial propagation of the large-scale magnetic field (Fig. 1); and (iv) solar-like differential rotation (fast at the equator, slow at the poles). Some nonsolar features were also produced, including the concentration of toroidal magnetic field at mid-rather than low latitudes, and an irregularly alternating pattern of symmetric and antisymmetric equatorial parity. This is apparent in Fig. 1D, where periods of symmetrical and antisymmetrical states follow one another. Such parity drifts are understood to reflect the interactions between the two families of dynamo symmetry (13–16), which couple in nonlinear regimes such as the one achieved in our experiment.

The magnetic cycle trends in our set of simulations are displayed in Fig. 2 (blue circles with error bars), where two main trends are identified. First, the magnetic cycle period (P_{cyc}) is found to decrease in proportion to the rotation rate when the convective luminosity is held constant (Fig. 2A). Second, the cycle period also decreases

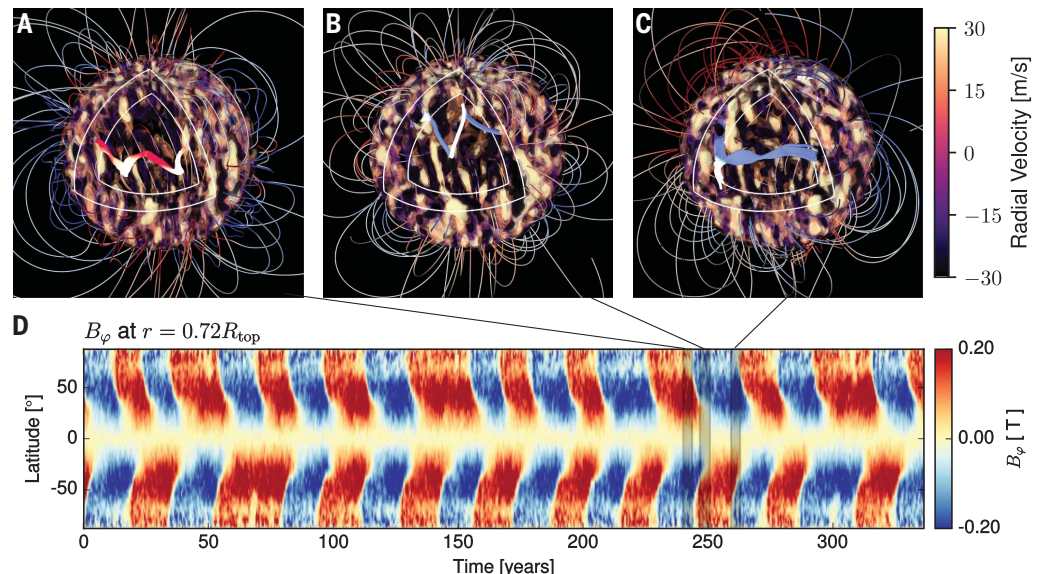
¹Département de Physique, Université de Montréal, C.P. 6128 Succursale Centre-Ville, Montréal, Québec H3C-3J7, Canada.

²Laboratoire Astrophysique, Instrumentation, Modélisation Paris-Saclay, Commissariat à l'Energie Atomique et aux Energies Alternatives/Irfu Université Paris-Diderot CNRS/ Institut National des Sciences de l'Univers, F-91191 Gif-sur-Yvette, Paris, France. ³Departamento de Física Teórica e Experimental, Universidade Federal do Rio Grande do Norte, CP 1641, 59072-970 Natal, Rio Grande do Norte, Brazil. ⁴Harvard-Smithsonian Center for Astrophysics, Cambridge, MA 02138, USA.

*Corresponding author. Email: antoine.strugarek@cea.fr

Fig. 1. A nonlinear, global magnetic cycle.

(A to C) Snapshots of a representative three-dimensional nonlinear simulation of a regular magnetic cycle. White (positive) and purple (negative) volumes represent the radial velocity (in meters per second) of the convective flow. A half sector of the spherical shell has been cut out to display the large-scale magnetic field lines (averaged over 50 rotation periods) buried in the convection zone (the red or blue coloring of the magnetic tubes labels positive or negative azimuthal magnetic field, respectively). The magnetic field lines extending beyond the simulation domain are derived from a standard potential field extrapolation (28). (D) Longitudinal average of the azimuthal component of the magnetic field (B_{ϕ}) as a function of latitude and time at depth $r = 0.72R_{\text{top}}$ (where R_{top} is the radius at the top of the spherical shell).



with increasing convective luminosity (L_{bc}) at constant rotation rate ($P_{cyc} \propto L_{bc}^{-0.8}$, see Fig. 2B and the supplementary materials for detailed definitions). When the results are converted to a nondimensional form (Fig. 2C) or when this luminosity dependency is compensated (Fig. 2D), our simulation results follow a single trend that matches the solar cycle.

We compare our results to the growing sample of observed magnetic cycles of distant stars in Fig. 2. A first sample was observed with Mount Wilson spectrophotometers (4, 5, 17). We added to this sample one star that was observed at the Lowell Observatory (18) and two stars observed using the HARPS (High Accuracy Radial Velocity Planet Searcher) spectrograph (19, 20). As the luminosities of these stars were not reported in the literature, we calculated these values by using parallaxes from the Gaia catalog (21, 22), V magnitudes, and a standard bolometric correction (23). The uncertainties on the Gaia parallaxes translate into luminosity uncertainties of <10% for most of the stars in the two samples. The samples are composed of stars with very different spectral types (from F to K) and, consequently, very different convection zone aspect ratios and luminosities. Some stars also exhibit two different cycle periods, in which case both periods are plotted in Fig. 2 and linked by a vertical dashed line.

Historically, two distinct branches in the rotation cycle period diagram (3, 5) have been favored in the literature. The Sun lies in between these branches (Fig. 2A), requiring conjecture that it is in a transition state between the branches (24). A third branch showing an anticorrelation between cycle period and rotation period was also identified for slower rotators (4). However, recent observations of solar-type stars seem to indicate a less clear picture that may not reduce to well-defined branches [e.g., orange diamonds in Fig. 2; also see (25)]. Our simulation results point to only one generic trend, in which the cycle period is inversely proportional to the rotation period. The dependence of the cycle period on the convective luminosity was not considered in earlier analyses of these stellar data and is shown to be responsible for part of the spread in the rotation cycle period diagram in Fig. 2, C and D, where the corrected cycle periods of the observed stars then form a broad band inversely proportional to the stellar rotation period, as suggested by our numerical simulations. We highlight three stars (HD 146233, HD 190406 and HD 7615; see table S2) that are likely to possess a convection zone of depth similar to that of the Sun. The observational sample still shows a spread around this trend, which is likely due to (i) the varying aspect ratio of the convection zone of the stars in the samples and (ii) the existence of multiple cycle periods for several stars.

The observed cycle period variations with stellar parameters have usually been interpreted through kinematic dynamo models formulated with mean-field theory (3, 4). The two key ingredients in such models are differential rotation and cyclonic turbulence, both resulting ultimately from the action of the Coriolis force on

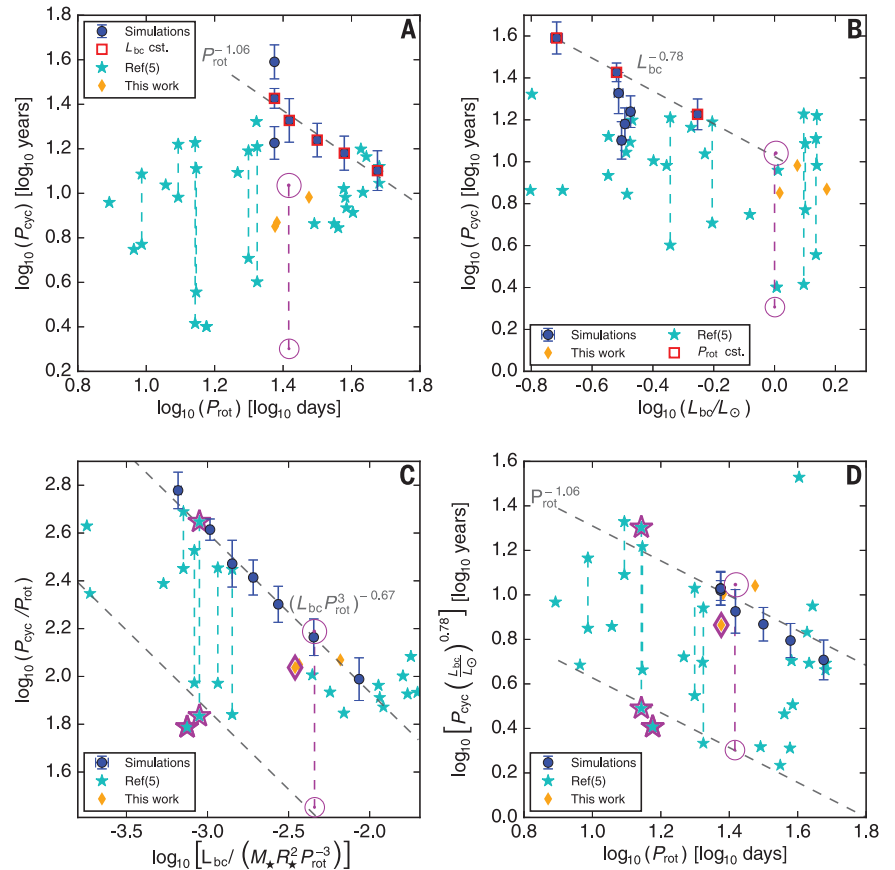


Fig. 2. Trends of the magnetic cycle period. The cycle half-periods (P_{cyc}) [11 and 2 years for the Sun (29–31), denoted by the purple \odot symbol] are plotted against the rotation period (P_{rot}) (A) and stellar luminosity (L_{bc}/L_{\odot} , where L_{bc} is convective luminosity and L_{\odot} is solar luminosity) (B) for our set of simulations (dark blue circles) and two observed samples of stars (light blue stars and orange diamonds) (4, 5). Red squares indicate models with constant luminosity (A) and constant, solar rotation rate (B) (cst., constant). (C) The same quantities represented in a normalized way, with the cycle period normalized to the rotation period and the luminosity normalized to $M_{\star}R_{\star}^2P_{rot}^{-3}$ (where M_{\star} and R_{\star} are the mass and the radius of the stars, respectively). Shapes with purple outlines represent stars possessing a convection zone with an aspect ratio similar to that of the Sun. The dependence of the cycle period upon the stellar convective luminosity observed in our set of simulations (B) is factored out in (D). In all panels, the best fit (using orthogonal distance regression) of our simulation data is shown by the gray dashed lines. Vertical dashed lines indicate stars that exhibit two different cycle periods. Error bars denote the variability of the cycle period in the simulations (see supplementary materials). Stellar data are available in table S2.

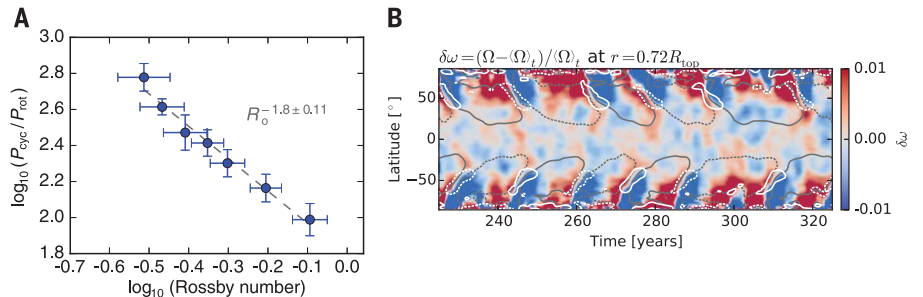


Fig. 3. Interpretation of the nonlinear convective dynamo. (A) Magnetic cycle period (normalized to the rotation period) as a function of the local Rossby number. The scaling law indicated by the dashed gray line is fitted with orthogonal distance regression. (B) Relative variation in time ($\delta\omega$) of the differential rotation as a function of latitude and time at depth $r = 0.72R_{top}$ (Ω is the differential rotation, defined as the azimuthal velocity divided by the cylindrical radius, and $\langle \rangle_t$ denotes the temporal average). The isocontours of the mean azimuthal magnetic field at ± 0.1 T are shown in gray. The contribution of shearing by differential rotation to the mean electromotive force is represented by white contours. Plain contours indicate positive contours, and dashed contours denote negative ones. All fields in (B) have been smoothed with a running average of 4 years, using a Hann window.

thermally driven convection. In this context, the governing parameter is the Rossby number (R_o), which measures the influence of rotation on the system (a small Rossby number corresponds to a fast-rotating state). The cycle period in our set of simulations is shown to scale as R_o^{-1} (Fig. 3), in contrast to dimensional inferences from a kinematic, linear mean-field dynamo (3), which instead predicts cycle periods proportional to R_o .

Our numerical simulations operate in a nonlinear regime in which the magnetic force alters the force balance sustaining the large-scale flows (10). In Fig. 3B, we show the systematic acceleration of the differential rotation that modifies the electromotive force to trigger the polarity inversion of the mean azimuthal magnetic field. The amplitude of these fluctuations in the differential rotation is small (~1%), similar to the ones observed on the Sun. A detailed analysis of our simulations (fig. S8) reveals that the torque applied by the large-scale magnetic field controls these modulations. The magnetic cycle period decreases when the amplitude of the differential rotation modulation increases, indicating that nonlinear feedback of the Lorentz force on the large-scale differential rotation is driving polarity reversals and setting the cycle period.

Although restricted in the stellar parameter range they span, our simulation results suggest a single trend of cycle period with rotational influence, quantified by the Rossby number, which can accommodate both the Sun and existing stellar data within a single dynamo branch, rather than multiple branches. The scatter about the mean relationship observed between cycle period and rotation rate (Fig. 2A) can be partly attributed to the sensitive dependence of the cycle

period on luminosity. The remaining scatter remains to be explained and could originate from structural factors such as the exact depth of the convection zone or the exact shape of the differential rotation, which have not been explored yet. These considerations reinstate the Sun to the status of an ordinary solar-type star and a robust calibration point for stellar astrophysics.

REFERENCES AND NOTES

1. S. L. Baliunas *et al.*, *Astrophys. J.* **438**, 269–287 (1995).
2. J. C. Hall, G. W. Lockwood, B. A. Skiff, *Astron. J.* **133**, 862–881 (2007).
3. R. W. Noyes, N. O. Weiss, A. H. Vaughan, *Astrophys. J.* **287**, 769–773 (1984).
4. S. H. Saar, A. Brandenburg, *Astrophys. J.* **524**, 295–310 (1999).
5. E. Böhm-Vitense, *Astrophys. J.* **657**, 486–493 (2007).
6. A. S. Brun, R. A. Garcia, G. Houdek, D. Nandy, M. Pinsonneault, *Space Sci. Rev.* **196**, 303–356 (2015).
7. H. Hotta, M. Rempel, T. Yokoyama, *Science* **351**, 1427–1430 (2016).
8. M. Ghizaru, P. Charbonneau, P. K. Smolarkiewicz, *Astrophys. J.* **715**, L133–L137 (2010).
9. P. J. Käpylä, M. J. Mantere, A. Brandenburg, *Astrophys. J.* **755**, L22 (2012).
10. K. Augustson, A. S. Brun, M. Miesch, J. Toomre, *Astrophys. J.* **809**, 149 (2015).
11. L. D. V. Duarte, J. Wicht, M. K. Browning, T. Gastine, *Mon. Not. R. Astron. Soc.* **456**, 1708–1722 (2016).
12. P. K. Smolarkiewicz, P. Charbonneau, *J. Comput. Phys.* **236**, 608–623 (2013).
13. A. Brandenburg, F. Krause, R. Meinel, D. Moss, I. Tuominen, *Astron. Astrophys.* **213**, 411–422 (1989).
14. D. Gubbins, K. Zhang, *Phys. Earth Planet. Inter.* **75**, 225–241 (1993).
15. S. M. Tobias, *Astron. Astrophys.* **322**, 1007–1017 (1997).
16. M. L. DeRosa, A. S. Brun, J. T. Hoeksema, *Astrophys. J.* **757**, 96 (2012).
17. R. W. Noyes, L. W. Hartmann, S. L. Baliunas, D. K. Duncan, A. H. Vaughan, *Astrophys. J.* **279**, 763–777 (1984).
18. J. C. Hall, G. W. Henry, G. W. Lockwood, *Astron. J.* **133**, 2206–2208 (2007).
19. M. Mayor *et al.*, *The Messenger* **114**, 20–24 (2003).
20. R. F. Diaz *et al.*, *Astron. Astrophys.* **585**, A134 (2016).
21. Gaia Collaboration *et al.*, *Astron. Astrophys.* **595**, A1 (2016).
22. Gaia Collaboration *et al.*, *Astron. Astrophys.* **595**, A2 (2016).
23. G. Torres, *Astron. J.* **140**, 1158–1162 (2010).
24. T. S. Metcalfe, R. Egeland, J. van Saders, *Astrophys. J.* **826**, L2 (2016).
25. V. See *et al.*, *Mon. Not. R. Astron. Soc.* **462**, 4442–4450 (2016).
26. F. Ochsenbein, P. Bauer, J. Marcout, *Astron. Astrophys. Suppl. Ser.* **143**, 23–32 (2000).
27. Astroquery package; <http://astroquery.readthedocs.io/en/latest/#>.
28. K. H. Schatten, J. M. Wilcox, N. F. Ness, *Sol. Phys.* **6**, 442–455 (1969).
29. S. T. Fletcher *et al.*, *Astrophys. J.* **718**, L19–L22 (2010).
30. R. Simoniello *et al.*, *Astrophys. J.* **765**, 100 (2013).
31. R. K. Ulrich, T. Tran, *Astrophys. J.* **768**, 189 (2013).

ACKNOWLEDGMENTS

We thank P. Smolarkiewicz for help and advice on using the EULAG code, J. F. Cossette for discussions about the modeling of convection inside stars, and R. Garcia for discussions on stellar rotation. We acknowledge support from Canada's Natural Sciences and Engineering Research Council. This work was also partially supported by the Institut National des Sciences de l'Univers/Programme National Soleil-Terre, the Agence Nationale de la Recherche 2011 Blanc Toupies, European Research Council grant STARS2 207430, and Centre National d'Etudes Spatiales Solar Orbiter and PLATO grants. This work made use of the VizieR database (26), through the Astroquery package (27). This work also made use of data from the European Space Agency mission Gaia (www.cosmos.esa.int/gaia), processed by the Gaia Data Processing and Analysis Consortium (www.cosmos.esa.int/web/gaia/dpac/consortium). The EULAG-MHD code can be accessed at www.astro.umontreal.ca/~paulchar/grps/eulag-mhd.html (subject to U.S. export restrictions). The simulation outputs are downloadable from www.astro.umontreal.ca/sun/, and the data for the stellar sample are tabulated in the supplementary materials.

SUPPLEMENTARY MATERIALS

www.sciencemag.org/content/357/6347/185/suppl/DC1
Materials and Methods
Figs. S1 to S9
Tables S1 and S2
References (32–45)

14 November 2016; accepted 5 June 2017
10.1126/science.aal3999

Reconciling solar and stellar magnetic cycles with nonlinear dynamo simulations

A. Strugarek, P. Beaudoin, P. Charbonneau, A. S. Brun and J.-D. do Nascimento Jr.

Science **357** (6347), 185-187.
DOI: 10.1126/science.aal3999

Is the Sun a solar-type star?

The Sun's activity, including sun-spot activity, varies on an 11-year cycle driven by changes in its magnetic field. Other nearby solar-type stars have their own cycles, but the Sun does not seem to match their behavior. Strugarek *et al.* used magnetohydrodynamic simulations to show that stellar activity periods should depend on the star's Rossby number, the ratio between the inertial and Coriolis forces. Turning to observations, they found that solar-type stars, including the Sun, follow this relation. The results advance our understanding of how stars generate their magnetic fields and confirm that the Sun is indeed a solar-type star.

Science, this issue p. 185

ARTICLE TOOLS

<http://science.sciencemag.org/content/357/6347/185>

SUPPLEMENTARY MATERIALS

<http://science.sciencemag.org/content/suppl/2017/07/12/357.6347.185.DC1>

REFERENCES

This article cites 43 articles, 1 of which you can access for free
<http://science.sciencemag.org/content/357/6347/185#BIBL>

PERMISSIONS

<http://www.sciencemag.org/help/reprints-and-permissions>

Use of this article is subject to the [Terms of Service](#)